e-ISSN: 2805-5756

PENERBIT PRESS
UNIVERSITI TEKNOLOGI MARA

Available online at
https://jaeds.uitm.edu.my

Journal of Applied Engineering Design and Simulation 6(2) 2026, 78-91

Journal of Applied Engineering Design and Simulation

One-way fluid-structure interaction analysis of oar blade designs: evaluating hydrodynamic performance and structural flexibility

Ab Aziz bin Mohd Yusof [1*], Amir Aziz[2], Akbar Teguh Prakoso[3], Fakhrizal Azmy Nasruddin[4]

[1]*Faculty of Mechanical Engineering, Universiti Teknologi MARA, Johor Branch, Pasir Gudang Campus, Masai, Malaysia*
[2]*Faculty of Mechanical and Automotive Engineering Technology, Universiti Malaysia Pahang Al-Sultan Abdullah, Pekan, Malaysia*
[3]*Department of Mechanical Engineering, Faculty of Engineering, Universitas Sriwijaya, Indralaya 30662, South Sumatra, Indonesia*
[4] *Department of Technical & Research, Summit Features Sdn Bhd, Kuala Lumpur, Malaysia*

ARTICLE INFO

Article history:
Received 16 March 2026
Revised 30 June 2026
Accepted 17 July 2026
Online first 30 September 2026
Published 30 September 2026

Keywords:
Rowing Blade
FSI
Fluid flow
Hydrodynamic pressure
Blade flexibility

DOI:
10.24191/jaeds.v6i2.184

ABSTRACT

Rowing propulsion relies on complex interactions between the paddle blade and the water, where blade design is crucial in determining efficiency and performance. During the stroke, the oar blade interacts with the water and undergoes structural deformation under hydrodynamic forces. In an actual situation, hydraulic forces and structural responses occur simultaneously, requiring FSI for study and evaluation. Thus, this study aims to evaluate the fluid-structure interaction (FSI) characteristics of three widely used paddle blades, Macon, Big, and Fat blade, using a one-way FSI approach. Computational Fluid Dynamics (CFD) was used to analyse the fluid flow and pressure distribution around the blade, while Finite Element Analysis (FEA) evaluated the structural deformation under hydrodynamic forces. Results revealed the Macon blade produced the lowest propulsive force of 326N at 90º blade position. The Big and Fat blade showed a force increase at 36% and 52%, respectively, compared to the Macon blade. In terms of structure, the Macon blade experienced tip deflection of 46.7mm, and the Big and Fat blade experienced bending with displacements of 11.5mm and 13.6mm, respectively, combined with twisting due to the rotational structure. The flexible blades, such as the Macon, offer smoother transitions and enhanced energy absorption. These findings underscore the importance of balancing blade stiffness, design, and hydrodynamic aspects to enhance rowing performance, offering valuable insights into optimizing paddle blade design

[1*]Corresponding author. *E-mail address*: abaziz86@uitm.edu.my

Nomenclature (Greek symbols towards the end)

k-ε	K-epsilon turbulence model
Cp	Propulsive coefficient

Abbreviations

FSI	Fluid-Structure Interaction
CFD	Computational Fluid Dynamics
FEA	Finite Element Analysis

1. INTRODUCTION

In rowing, propulsion is a critical element of sports engineering, where hydrodynamic force is generated by the rowers through their oars, propelling the boat forward [1]. In competitive race events, rowing performance depends on how effectively rowers apply force to the water through their oars, creating the necessary hydrodynamic forces to accelerate the boat [2-5]. The interaction between the oar blade and the water is pivotal in determining the efficiency of this force generation, making it essential to explore its effects on hydrodynamics. Various oar blade designs are available, each with unique performance characteristics [6]. Curved blades, for instance, maximise water displacement, providing better grip and improving propulsion with each stroke [7-9]. Additionally, a larger blade surface increases the volume of water displaced, leading to more efficient energy transfer and ultimately contributing to greater speed and performance in rowing. However, a larger blade may increase drag, so an optimal balance must be achieved.

Propulsive force is generated during the rowing stroke as the blade travels from the catch to the finish. According to a study, the catch angle varied between 40° and 80° during the stroke [10]. As the blade moves along the stroke path, it produces a hydrodynamic force profile, with maximum forces reported to range between 100 and 393 N [11-13]. Research by W. van Nieuwburg et al. (2023) demonstrated that improvements in blade design significantly enhance force generation. A higher force output was achieved by tilting the blade at a 15-degree angle relative to the oar, thus improving performance [7]. Additionally, increasing the blade area has a positive impact on the force generated, ultimately contributing to higher boat speed [7].

In a more detailed study, E. Grift et al. (2021) analysed the composition of forces acting on the blade and fluid flow around it. The forces were categorised into six components, each defined by axes relative to the oar blade, boat motion, and the reference flow velocity [10]. The kinematics of the blade path influence these forces, with the highest force observed when the blade is perpendicular to the boat's direction [10]. Throughout the stroke, the drag force is most dominant during the middle of the drive phase, while the lift force predominates at the start, gradually diminishing towards the finish. Vortex formation occurs around the blade during the stroke and affects the force profile [10, 11]. A leading-edge vortex, identified at the blade tip during smaller stroke angles, pushes away toward the finish. A swirling region characterises the vortex as a pressure difference near the leading edge due to fluid wrapping phenomena [11]. Blade performance can be further optimised by altering its design [14], such as increasing blade width or adding additional foils to modify flow characteristics further.

The strength and flexibility of the oar blade are critical factors in optimising rowing performance. The interaction between blade hydrodynamics and its structural flexibility is essential for enhancing efficiency. A study by M. Hofmijster et al. (2010) compared flexible and rigid oars, revealing that ignoring flexibility leads to an underestimation of force at the beginning and end of the stroke and an overestimation in the middle. This finding is supported by research from A. Sliasas and S. Tullis (2011) [15, 16]. A stiffer oar structure is recommended for improved performance, as flexibility can reduce efficiency by up to 4% due to bending and associated blade lag, especially on the handle side [17]. While flexibility can store energy released later in the stroke, excessive flexibility may be disadvantageous. There are several studies exploring the sport performance, especially rowing, using the FSI approach [3, 18]. In the study by A. Leroyer et al. (2019), a boat-oar-rower was developed to investigate the interaction between water hydrodynamics and fluid-structure interaction arising from the movements of the whole boat and the system's flexibility [18].

Regarding the aforementioned subjects, this study aimed to investigate fluid-structure interaction (FSI) between water and the commonly used competitive rowing blades: Fat, Big, and Macon. Numerical simulation techniques were employed, specifically Computational Fluid Dynamics (CFD) and Finite Element Analysis (FEA). CFD was utilised to examine the fluid flow around the different blade designs, while FEA assessed the structural integrity of the blades under hydrodynamic forces. These two approaches were integrated using the software's One-Way FSI capabilities, which solved both fluid dynamics and structural mechanics equations with one-directional influence, with fluid forces acting on the structure. However, structural deformation did not feed into the fluid flow.

2. METHODOLOGY

2.1 Blade geometries

Three competitive rowing oar blade geometries were investigated in this study, namely the Macon, Big, and Fat blades. These designs represent commonly used blade configurations in rowing competitions and were selected to evaluate the influence of blade shape and surface area on hydrodynamic performance and structural response. The three-dimensional CAD models were developed using SolidWorks, and the blade geometries are shown in Figure 1.

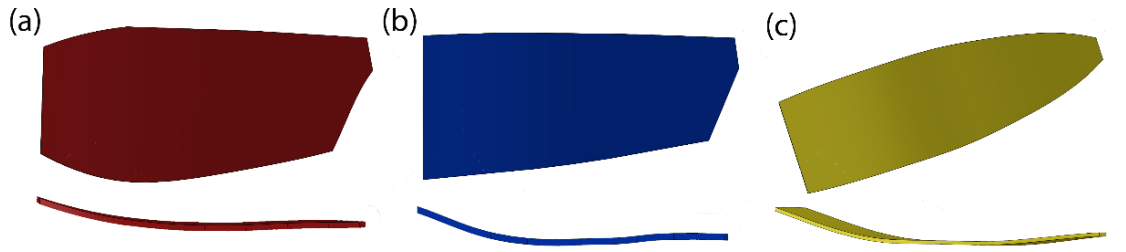


Fig 1. Oar blade models (a) Fat blade (b) Big Blade (c) Macon blade

The Macon blade features a traditional elliptical shape that is narrower and longer, optimised for smooth water entry and consistent stroke control, as shown in Figure 1(a). The Big Blade (Figure 1(b)) features a broader, more squared shape than the Macon, allowing greater power per stroke due to its increased surface area, making it ideal for higher stroke rates. The Fat blade (Figure 1 (c)) is the broadest of the three, providing the maximum surface area to enhance water grip, power, and speed, although it demands more strength and a refined rowing technique than the narrower blades. The general dimensions of the blades are provided in Table 1. Each blade was modelled with curvature along its longitudinal axis, with a greater bend near the tip to enhance water grip during the stroke.

Table 1: General dimensions of the blades

Blade type	Length (m)	Width (m)	Area (m^2)
Fat	0.587	0.276	0.137
Big	0.5633	0.256	0.124
Macom	0.540	0.171	0.090

2.2 Boundary conditions

This study conducted CFD and FEA simulations separately using the SolidWorks software package provided by the developer. The study began with CFD, followed by the transfer of fluid loads to the structural simulation using FEA for fluid-structure interaction (FSI) analysis. Two sets of boundary conditions were required, as illustrated in Figure 2. The specific boundary conditions for both the CFD and FEA simulations are detailed in separate sections.

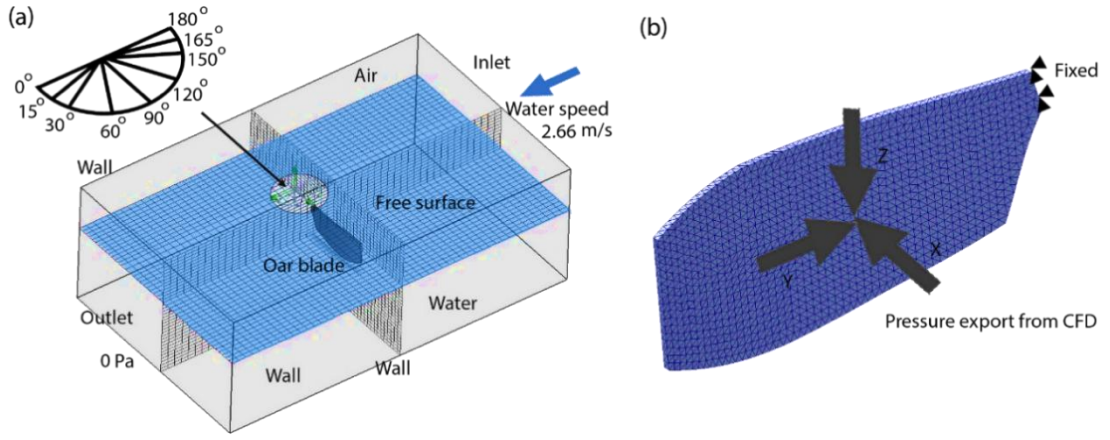


Figure 2. Boundary condition of the computational study for FSI (a) Computational fluid dynamics (b) Finite element analysis of the blade

2.3 Computational fluid dynamics

The CFD boundary conditions are shown in Figure 2(b). A water flow rate of 2.66 m/s was applied at the inlet of the domain, while a pressure of 0 Pa was assigned at the outlet, generating pressure as water impacted the blade. The domain's left, right, and bottom surfaces were set as walls with slip conditions, allowing water to slide along these surfaces without friction, thereby eliminating tangential stress at the boundaries.

To simulate real-world conditions in which the blade operates near the water surface, an air-water interface was included to account for free-surface effects. Gravity was applied with an acceleration of 9.81 m/s^2 downward. The simulation defined the fluid properties using an External Immiscible Liquid model: water at room temperature had a density of 999.79 kg/m^3 and dynamic viscosity of 0.0017912 Pa·s, while air had a density of 1.24 kg/m^3 and viscosity of 1.85×10^{-5} Pa·s. The External Immiscible Liquid model is a multiphase model used to define a non-mixing fluid between air and water. The clear interface between them is known as freesurface, which later acts as a wave around the moving oar blade. The study used the k-ε turbulence model for fluid flow analysis, as it offers a balance between computational accuracy, calculation effectiveness, and robustness. Besides, this model is suitable for the external flow problem as this flow is bonded with the wall.

The computational domain was set to 2 m (width) × 3.2 m (length) × 1.1 m (height) to minimise wall effects as the fluid flowed from the inlet to the outlet and interacted with the blade. The blade was positioned at the centre of the domain at nine orientations ranging from 0° to 180° (see Figure 2) as the parameters of the quasistatic study, eliminating the blade's momentum. The simulation ran for a maximum physical time of 10 seconds in a time-dependent analysis.

The CFD analysis focused on determining the pressure distributions of the water mass fraction, flow trajectories, and free surface isosurfaces. It also measured the propulsive force generated on the blade surface by integrating the forces over the blade's projected area perpendicular to the flow. All key results were extracted automatically using the software's goal-setting feature.

2.4 Finite element analysis

The blade was fixed at the corner connecting to the oar shaft, as shown in Figure 2(b). The pressure for Fluid loads data obtained from the CFD analysis, including fluid shear stresses along the X, Y, and Z axes, was transferred to the FEA simulation as fluid pressure inputs. The study was conducted for three different blade models, similar to a CFD study. The blade material was modeled as a fiberglass-reinforced resin, treated as a linear elastic, isotropic material with an elastic modulus of 9.7×10^{10} N/m^2, Poisson's ratio of 0.3, density of 1960 kg/m^3, and yield strength of 2.5×10^9 N/m^2 [19].

The structural analysis was conducted using a static analysis approach with large displacement settings, treating the blade as a solid body. This analysis assessed the blade's flexibility by evaluating its bending response under fluid forces based on the resulting stress distribution and displacement. The goal is to understand how applied hydrodynamic forces influence structural behaviour, particularly the extent of deformation, which is crucial for optimizing blade performance.

2.5 Numerical study of propulsive

According to previous studies by N. Caplan et al. (2007) and N. Caplan (2010), the propulsive force generated by a rowing blade can be calculated using the relative speed between the boat and the oar blade, the blade's projection area, the density of water, and a propulsive coefficient, as shown in equation 1 [20, 21].

$$Propulsive\ force, F_p = \frac{C_p \rho {v_r}^2 A_o}{2} \quad \text{(N)} \quad (1)$$

For this study, the Fat blade model, positioned at 90°, was chosen for calculation because it is expected to produce the highest magnitude. The propulsive coefficient, $C_{p,}$ was set to 1.33, with water density assigned to CFD of 999.79 kg/m³. The initial fluid flow test revealed a 13% decrease in velocity from the inlet speed of 2.6 m/s, resulting in the water striking the blade at 2.3 m/s. The blade's perpendicular projection area was 0.1371 m². Using these parameters, the calculated propulsive force was 482 N. The propulsive force is predicted to decrease as the blade angle changes due to variations in the effective projection area.

2.6 Mesh convergence study

A mesh convergence study was conducted for CFD and FEA to ensure the accuracy of the results. As illustrated in Figure 3(a), increasing the number of elements in the CFD analysis gradually decreased the force generated on the blade until it reached a converged value. Similarly, Figure 3(b) shows the FEA convergence study for the solid blade; as the mesh density increased, the von Mises stress converged.

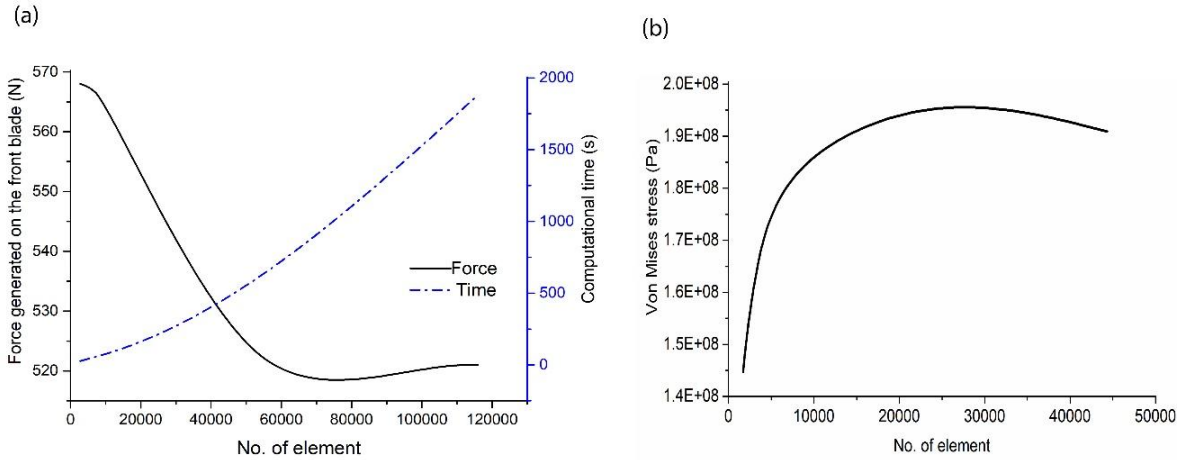


Figure 3. Mesh convergence studies (a) Computational fluid dynamics (b) Finite element analysis

The fluid domain was meshed using hexahedral elements, as shown in Figure 2(a). The force generated on the blade increased by 8% when comparing results from the lowest tested mesh count (2,747 elements) to the highest converged mesh count (115,895 elements), as shown in Figure 3(a). However, computational time increased by 6,600%, from 28 seconds to 1,878 seconds. After balancing force accuracy and computational efficiency, a mesh size of 80,000 elements was chosen to further analyse all blade positions and designs. This mesh configuration achieved a perfect aspect ratio score, with 100% of elements having an aspect ratio below 3.

The solid blade was meshed using tetrahedral elements for the FEA, as seen in Figure 2(b). A consistent mesh size was applied across the entire blade, resulting in nearly uniform computational times of about 40 seconds for all blade positions, indicating that computational time was not a limiting factor for FEA. Figure 3(b) depicts that von Mises stress increased by 32% from the coarsest to the finest mesh. Based on these results, a mesh size of 20,000 elements was selected for subsequent analyses of various blade models and orientations.

3. RESULTS

The propulsive force generated by the blade was compared with the theoretical value calculated using Equation 1 for validation. The CFD results showed a 2.63% difference from the calculated value, which is considered highly acceptable for further analysis. The CFD-projected propulsive force was 495 N, while the calculated force was 482 N. The slight difference is likely due to the blade curvature, which is not accounted for in the theoretical calculation. It is suggested that a minor adjustment to the propulsive coefficient could improve the accuracy of the results.

Further analysis was conducted for different blade positions and types, as shown in Figure 4. Hydrodynamic forces were extracted from both the front and back of the blade. The Macon blade generated the lowest forces across all positions, with the highest force of 326 N occurring at the 90° position. Both the Big and Fat blades maintained almost similar propulsive forces, but the maximum forces were increased by 36% and 52%, respectively, compared to the Macon blade. The hydrodynamic forces showed a different pattern on the back of the blade. The ratio of maximum force generated per unit area was 3,622 N/m², 3,580 N/m², and 3,613 N/m² for the Macon, Big, and Fat blades, respectively.

The hydrodynamic force acting on the back surface of the blade was extracted, as illustrated in Figure 4. The analysis revealed that the force magnitude was approximately 100 N, as the back surface does not directly affect the water. The force was calculated using the same method applied to the front blade, integrating the pressure over the back blade's surface area. Unlike the front blade, the force pattern showed four distinct peaks at 0°, 60°, 120°, and 180°. The force generated on the back side was proportional to the force generated on the front side.

Among the three blade designs studied, the Fat blade exhibited the highest hydrodynamic force, peaking at 130 N at a blade position of 180°, with an average force of 55 N across all positions. This was followed by the Big blade, which reached a maximum force of 120 N at 180° and had an average force of 41 N. The Macon blade had the lowest values, with a peak force of 97 N at 180° and an average force of 30 N.

Further analysis of the fluid flow around the blades was conducted, as shown in Figure 5. A flow projection at a 90° blade position was examined, as this position produced the highest hydrodynamic force. In general, a blade can be defined by four sides: the blade neck (where it attaches to the shaft), the blade tip (opposite the neck and the farthest point), the top side (closest to the water surface), and the bottom side (deepest submerged side).

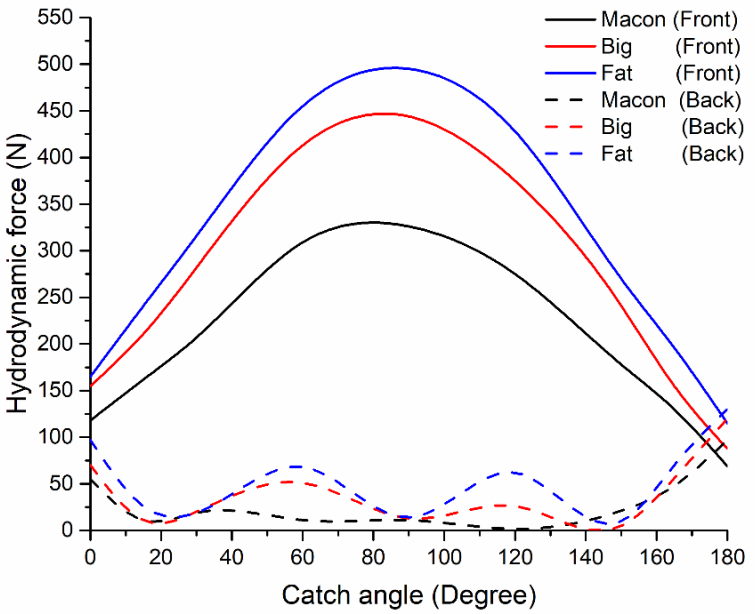


Figure 4. Hydrodynamic force generated on the blade: Front and back blade for all the blade models

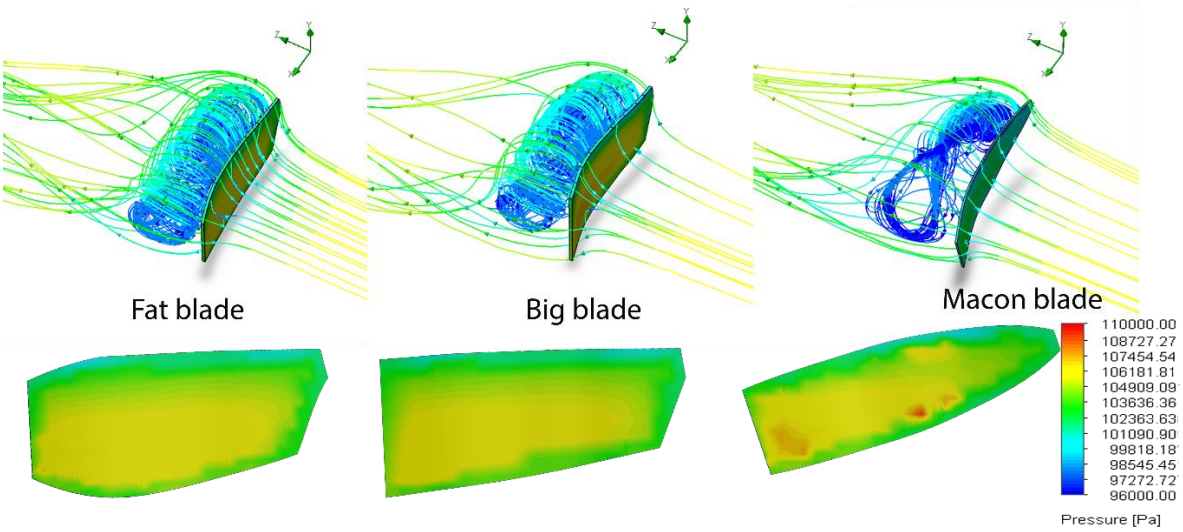


Figure 5. Vortex formation around the blades as water passes and pressure contours at a 90-degree position for the Macon, Big, and Fat blades.

For the Macon blade, the flow analysis revealed wake formation and flow separation at the rear of the blade, leading to a vortex that circulated from the blade neck to the tip. In contrast, for the Big and Fat blades, the water flow generated vortices that circulated from the top to the bottom, creating a region of lower velocity and higher turbulence, which eventually increased drag on the blades. The average water circulation speeds behind the blades were recorded as 0.649 m/s for the Macon blade, 0.636 m/s for the Fat blade, and 0.627 m/s for the Big blade. According to the pressure distribution shown in Figure 5, the highest pressure was observed near the blade's tip on its bottom side. The Macon blade exhibited an average pressure of 110,586 Pa, with a maximum of 115,091 Pa. For the Big blade, the average pressure was 105,564 Pa, with a peak pressure of 108,487 Pa. Meanwhile, the Fat blade showed an average pressure of 106,181 Pa, reaching a maximum of 108,727 Pa.

Based on the quasistatic projection, the pressure contour on the blade's front side is illustrated in Figure 6. The generated pressure varied with the angle as the blade moved through positions from 0° to 180°. At angles below 60°, the highest pressure was concentrated near the blade neck, where the flow first impinged on the blade, reaching a maximum of 104,404 Pa. As the blade reached a perpendicular orientation to the water flow (90°), the flow impacted the entire blade surface, resulting in a maximum pressure of 106,941 Pa, covering most of the blade area, as shown in Figure 6. Beyond 90°, as the blade angle increased, water struck the blade tip directly. This caused the pressure distribution to become more concentrated toward the blade tip, with a maximum pressure of 107,775 Pa observed there. The hydrodynamic pressure exerted on the blade's front surface was transferred to its structure, causing it to bend, as illustrated in Figure 7. This bending pattern reflected the blade's flexibility, which could have influenced boat performance by affecting how force was transferred from the blade to the oar shaft, oarlock, and, ultimately, the boat shell's acceleration.

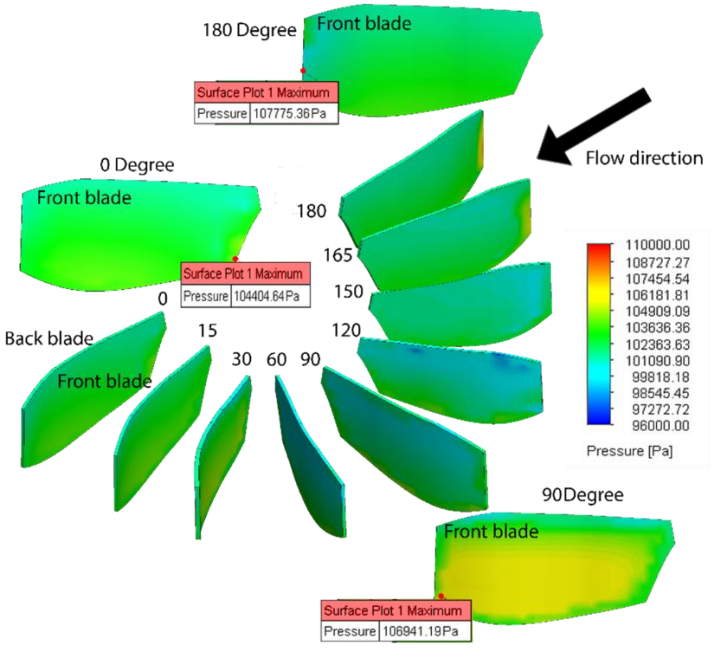


Figure 6. The blade position used in the study varied from 0 to 180 degrees. Three blade positions were highlighted: 0, 90, and 180 degrees.

The analysis revealed that the highest von Mises stress was concentrated near the blade neck. Among the designs studied, the Macon blade experienced the highest stress levels, with a maximum von Mises stress of 3.7 × 10^8 Pa, primarily due to greater bending. This stress value was approximately 21% higher than that of the Big blade and nearly 100% higher than that of the Fat blade, indicating a significant increase in stress due to the Macon blade's structural flexibility.

Similar to the stress distribution, the Macon blade exhibited the greatest bending deformation. The structural analysis revealed that, under applied pressure, the Macon blade bent backward with a small rotational displacement, reaching a maximum tip deflection of 46.7 mm. In contrast, the highest hydrodynamic pressure was concentrated on the lower side of the blade for both the Big and Fat blades, as shown in Figure 5. This uneven pressure distribution led to asymmetric forces, resulting in bending and rotational displacement of these blades. Specifically, the Big blade experienced backward bending with a tip displacement of 11.5 mm and some rotational movement. The Fat blade showed even greater deformation, with a tip displacement of 13.6 mm and a larger rotational angle than the Big blade.

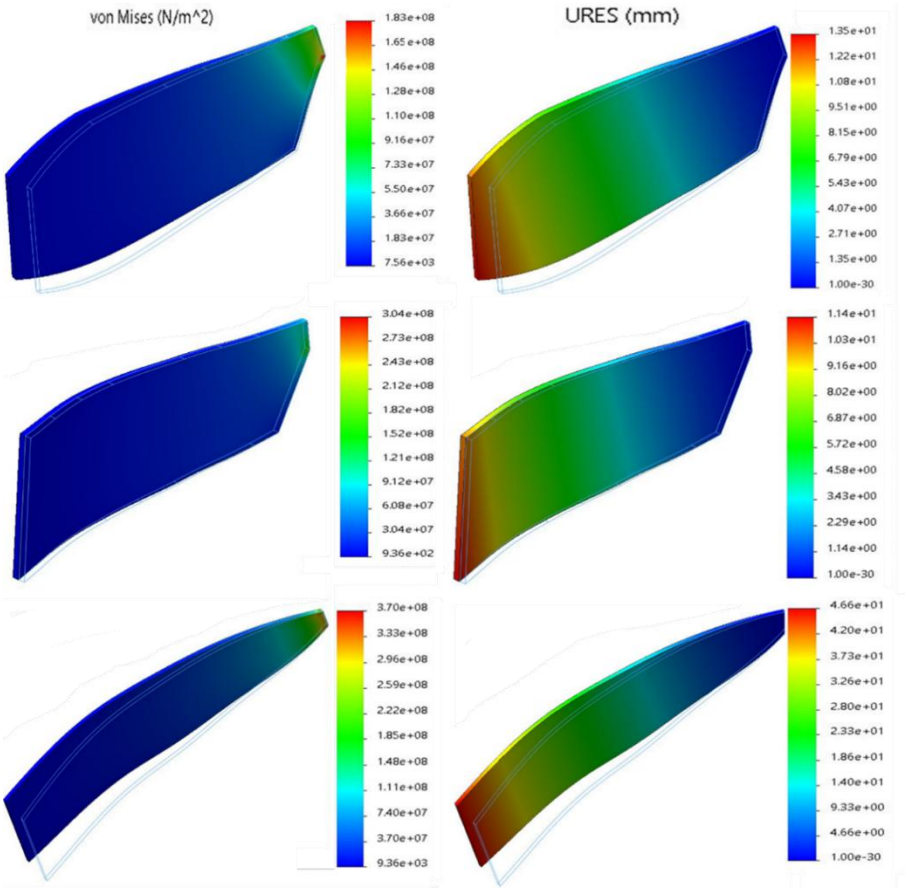


Figure 7. Blade deformation in von Mises stress and bending displacement due to hydrodynamic force imported from CFD.

4. RESULTS AND DISCUSSION

Pressure distribution on the blade reveals the location of the applied force. Most of the hydrodynamic forces act on the lower side of the blade, creating a torque bending moment on the oar structure. A study by M. Qi et al. (2023) on flapping structures highlighted the effects of torsional and bending stiffness on performance [22]. For the oar blades, the torsional stiffness plays a significant role in their interaction with water. Similar to how increased torsional stiffness reduces passive rotation in wings, a stiffer oar blade minimises unwanted deformation during the stroke, particularly for blades with a larger surface area. A stiffer blade maintains a more consistent angle of attack relative to the water, thereby enhancing the generation of hydrodynamic force throughout the stroke. Conversely, more flexible blades, such as those made by Macon, tend to bend under load. This deformation alters the effective angle of attack and may reduce stroke efficiency, thereby reducing the effective force transmission during rowing.

The swirling water forms rotating vortices, creating a pattern of alternating low-pressure zones behind the blade. This vortex flow, also known as wake turbulence, increases drag on the blade and can affect its lift. The blade design plays a crucial role in controlling these vortices. More streamlined shapes, such as the Fat and Big blades, minimize turbulence, reducing unwanted drag and improving propulsion efficiency. In contrast, symmetrical designs like the Macon blade may generate more wake turbulence, which impacts performance.

Flexible blades significantly impact the propulsive force generated and the boat's acceleration, but their performance depends on proper tuning to ensure a proper fit and optimal performance. Acting like a spring, these blades absorb energy early in the stroke and release it near the end. This flexibility, reflected in the blade flex, facilitates a smoother transition between the catch (when the blade first enters the water) and the drive phase (the power phase of the stroke). This smoother movement reduces the "shock" or sudden load on the rower's muscles and joints, making each stroke feel lighter and more efficient, especially beneficial for maintaining performance over longer distances.

Additionally, the blade's flexibility allows small adjustments in angle and position during water interaction, potentially enhancing grip and stability. Among the three blade designs, the Macon blade, with its symmetrical shape, is the most flexible, allowing significant flex but reducing rowing efficiency. The Fat blade exhibits superior performance compared to the Big and Fat blades by bending more effectively under higher impact forces, thereby improving efficiency and overall propulsive contribution.

Most previous studies have focused on measuring oar bending to assess performance, including blade, inboard, and outboard shaft [16, 23, 24]. One of the studies done by M. N. Macrossan (2008) typically evaluated the stiffness through the deflection of the oar under a dead weight of 10 kg (approximately 98 N) applied 2.05 meters from the gate (considered the fixed location) [17]. This approach classifies oars into two categories: medium and high stiffness. The same classification can also be applied to blade bending.

The blade's flexibility can be evaluated using angular deflection, derived from the maximum linear deflection of a cantilever beam, expressed as $\delta=Pl^3/3EI$, where P is the load on the blade, ℓ is the length of the blade, E is the elastic modulus of the fiberglass material, and I is the moment of inertia of the blade's cross-section. This equation can be further related to angular deflection using $\phi=Pl^2/2EI$. By relating angular deflection to linear deflection, it simplifies to $\phi=1.5\delta/l$ Using the derived equation, the angular deflection values for each blade type were calculated as follows: the Macon blade exhibited a deflection of $\phi = 0.129$ rad (7.42 º). While the Fat blade is shown $\phi = 0.035$ rad (2.00 º), and the Big blade limit $\phi = 0.030$

rad (1.71 º). Based on these results, the Macon blade is classified as having medium stiffness, as its deflection angle exceeds 5 degrees, indicating greater flexibility. In contrast, the Big and Fat blades fall into the high-stiffness category due to their relatively low angular deflections, indicating greater rigidity in their current designs.

High-stiffness blades are more efficient at transferring force with minimal bending, potentially enhancing rowing performance, but may require more effort from the rower [16]. In contrast, medium-stiffness blades, such as the Macon, strike a balance by offering some flexibility to absorb shocks while maintaining effective force transfer. This additional flexibility can provide a smoother rowing experience, although it may slightly reduce force transfer efficiency to the boat.

5. CONCLUSIONS

The findings show that blade design has a significant impact on hydrodynamic performance and structural behaviour during rowing. Fat blades produce the highest propulsive force due to their larger surface area, while Macon blades exhibit the highest flexibility, resulting in greater bending deformation and reduced force output. Hydrodynamic forces acting on the blade indicate that the lower surface experiences the highest stress, leading to torques and bending moments that vary with the blade design and stiffness. Fat and Big blades exhibit a more streamlined design, minimizing wake turbulence and increasing propulsive efficiency compared to the symmetrical Macon blades. However, the flexibility of the Macon blade provides a smoother force transition, which may reduce rower fatigue during prolonged use. Structural analysis highlights the critical role of stiffness: stiffer blades exhibit minimal deformation and efficient force transfer but require greater physical effort.

In contrast, medium stiffness blades such as the Macon offer better energy absorption and smoother handling, but at the cost of reduced efficiency. This study emphasizes the need to balance hydrodynamic performance, structural durability, and rower effort when designing paddle blades. Future research could focus on optimizing blade geometry and material properties for specific rowing conditions to further improve performance and efficiency.

6. ACKNOWLEDGEMENTS/FUNDING

All the authors would like to thank all members and lecturers who helped complete the project and this journal.

7. CONFLICT OF INTEREST STATEMENT

No conflict of interest was disclosed.

8. AUTHORS' CONTRIBUTIONS

Ab Aziz bin Mohd Yusof: Conceptualization, Methodology, Validation, Writing - Original Draft, Amir Aziz: Writing - Review & Editing, Akbar Teguh Prakoso: Manuscript editing, Fakhrizal Azmy Nasruddin: Formal analysis.

9. DECLARATION OF GENERATIVE AI IN THE WRITING PROCESS

During the preparation of this work, the authors used Gemini to draft the introduction and to improve the manuscript's overall readability and language quality. After using this tool and its services, the authors reviewed and edited the content as needed and take full responsibility for the publication's content.

10. DATA AVAILABILITY/SUPPLEMENTARY MATERIALS

The datasets used and analysed in this study are available upon request.

11. ETHICS STATEMENT

The authors declare that this research did not involve human or animal subjects. All methodology procedures were performed following numerical study, computational modeling, and software simulation. To ensure academic integrity and reproduction of the reported data, all the simulation parameters used, assigned material, and boundary conditions have been reported in detail within this journal

12. REFERENCES

[1] M. N. Harun, F. A. Nasruddin, and A. Syahrom, "Rowing biomechanics, physiology and hydrodynamic: A systematic review," International journal of sports medicine, vol. 43, no. 07, pp. 577-585, 2022.

[2] N. Legge, C. Draper, K. Slattery, D. O'Meara, and M. Watsford, "On-water Rowing Biomechanical Assessment: A Systematic Scoping Review," Sports Medicine-Open, vol. 10, no. 1, p. 101, 2024.

[3] A. A. Mohd Yusof, M. N. Harun, and A. Syahrom, "Computational Fluid Dynamic of Rowing Using Fluid-Structure Interaction," in Rowing Biomechanics and Hydrodynamics: Performance Enhancement Through Sport Engineering: Springer, 2025, pp. 47-53.

[4] A. Thompson, Rowing Power. Publifye AS, 2025.

[5] F. A. Nasruddin et al., "Biomechanical Influence of Anthropometry on Stroke Technique and Power Output in Malaysian Elite Rowers: A Motion and Force Analysis Approach," Gait & Posture, vol. 121, pp. 159-161, 2025.

[6] V. Kleshnev and E. Andreeva, "Determining the effectiveness of oar blades in rowing," Theory and Practice of Physical Culture, no. 9, pp. 21-23, 2025.

[7] W. van Nieuwburg et al., "Improving rowing performance by adjusting oar blade size and angle," Frontiers in Sports and Active Living, vol. 5, p. 1109494, 2023.

[8] R. Cardoso et al., "Mechanics and energetic analysis of rowing with Big blades with Randall foils," International Journal of Sports Medicine, vol. 44, no. 14, pp. 1043-1048, 2023.

[9] V. Kleshnev, "Efficiency of various blade types in rowing," Sports Biomechanics, pp. 1-11, 2026.

[10] E. Grift, M. Tummers, and J. Westerweel, "Hydrodynamics of rowing propulsion," Journal of Fluid Mechanics, vol. 918, p. A29, 2021.

[11] A. Yusof, A. H. Omar, A. Syahrom, and M. Harun, "Analysis of oar blade hydrodynamics for rowing propulsive mechanism: Experiment and computational fluid dynamics simulation," International Review of Mechanical Engineering, vol. 12, pp. 920-927, 2018.

[12] A. Sliasas and S. Tullis, "A hydrodynamics-based model of a rowing stroke simulating effects of drag and lift on oar blade efficiency for various cant angles," Procedia Engineering, vol. 2, no. 2, pp. 2857-2862, 2010.

[13] B. Elliott, A. Lyttle, and O. Birkett, "Rowing: The RowPerfect Ergometer: a training aid for on-water single scull rowing," Sports Biomechanics, vol. 1, no. 2, pp. 123-134, 2002.

[14] R. Cardoso et al., "Effect of Randall foils on the rowing propulsive cycle," Sports Biomechanics, pp. 1-10, 2024.
[15] M. Hofmijster, J. De Koning, and A. Van Soest, "Estimation of the energy loss at the blades in rowing: common assumptions revisited," Journal of sports sciences, vol. 28, no. 10, pp. 1093-1102, 2010.
[16] A. Sliasas and S. Tullis, "Modelling the effect of oar shaft bending during the rowing stroke," Proceedings of the Institution of Mechanical Engineers, Part P: Journal of Sports Engineering and Technology, vol. 225, pp. 265-270, 12/01 2011, doi: 10.1177/1754337111408187.
[17] M. N. Macrossan, "The direction of the water force on a rowing blade and its effect on efficiency," 2008.
[18] A. Leroyer et al., "Fluid-Structure Interaction and High-Performance Computing to serve sport performance in rowing," in 24ième Congrès Français de Mécanique, CFM 2019, 2019.
[19] L. C. Pardini and L. G. B. Manhani, "Influence of the testing gage length on the strength, Young's modulus and Weibull modulus of carbon fibres and glass fibres," Materials research, vol. 5, pp. 411-420, 2002.
[20] A. Coppel, T. Gardner, N. Caplan, and D. Hargreaves, "Simulating the fluid dynamic behaviour of oar blades in competition rowing," Proceedings of the Institution of Mechanical Engineers, Part P: Journal of Sports Engineering and Technology, vol. 224, no. 1, pp. 25-35, 2010.
[21] N. Caplan and T. N. Gardner, "A fluid dynamic investigation of the Big Blade and Macon oar blade designs in rowing propulsion," Journal of sports sciences, vol. 25, no. 6, pp. 643-650, 2007.
[22] M. Qi, W. Zhu, and S. Li, "The Effect of Torsional and Bending Stiffness on the Aerodynamic Performance of Flapping Wing," Aerospace, vol. 10, no. 12, p. 1035, 2023. [Online]. Available: https://www.mdpi.com/2226-4310/10/12/1035.
[23] B. Laschowski, C. C. Hopkins, J. R. de Bruyn, and V. Nolte, "Modelling the deflection of rowing oar shafts," Sports Biomechanics, vol. 16, no. 1, pp. 76-86, 2017.
[24] H. Alkhraisat, "Optimization of high modulus carbon oar-shaft using grey wolf optimizer," Arabian Journal for Science and Engineering, vol. 48, no. 2, pp. 2041-2060, 2023.



© 2026 by the authors. Submitted for possible open access publication under the terms and conditions of the Creative Commons Attribution (CC BY-NC-ND) license (http://creativecommons.org/licenses/by/4.0/).